Available online at www.sciencedirect.com

SciVerse ScienceDirect

Journal of the European Ceramic Society 32 (2012) 2935–2948

www.elsevier.com/locate/jeurceramsoc

Atomistic modeling of the effect of codoping on the atomistic structure of interfaces in α-alumina

Abhishek Tewari *, Sandra Galmarini, Michael Stuer, Paul Bowen

Laboratoire de technologie des poudres, École Polytechnique Fédérale de Lausanne, 1015 Lausanne, Switzerland

Available online 23 March 2012

Abstract

Sintering aids or dopants have often been used successfully to limit the grain growth of alumina during sintering. Recently codoping of alumina with transition elements has been reported to produce additional effects in comparison to single doping in enhancement of creep and real in-line transmittance of light. The current study attempts to address the issue of the atomistic mechanism behind these experimentally observed codoping effects. The effect of codoping on the atomistic structure of a series of La–Y, Mg–Y, La–Mg codoped α-alumina interfaces was studied using energy minimization calculations. The segregation energy for single doping as well as codoping is negative for all the surfaces and grain boundaries. While, there is no significant energetic gain for La–Y cosegregation in comparison to single doping whereas segregation energies for Mg–Y and Mg–La codoping is more negative than single doping. A specific arrangement of dopants (associative effect) is also observed in La–Y codoped interfaces. Both mechanisms can thus contribute to the improved microstructures and properties.

Keywords: Grain boundaries; Impurities; Interfaces; Al_2O_3; Atomistic modeling

1. Introduction

Since the discovery of translucent polycrystalline alumina (LucAlOx) by Coble[1] in 1962, efforts have been made to achieve transparent polycrystalline alumina in many research groups for the last few decades.[2–5] In addition to its excellent mechanical properties and chemical stability at high temperatures, the possibility of large flat sheets and curved shapes makes it a potential material for a wide variety of transparent applications; e.g. watches, jewelry, wave guides, armors, high temperature windows[6] and metal–halide lamps.[7] It has been well established that fully dense (99.99%) ultrafine grained alumina is necessary to achieve high real in-line transmittances (RITs) due its birefringence.[3,5,8] Therefore, it is necessary to achieve maximum densification with minimum grain growth in the final stages of sintering. Various rare earth elements (La, Mg, Y) have been employed in the literature as sintering aids/dopants for the sintering of transparent alumina.[4,5,9] These dopants segregate to the grain boundaries, thereby reducing the rate of densification as well as grain size/sintered density ratio.[10,11] Recently, codoping of alumina with rare earth elements (e.g. La–Y, Y–Mg, Mg–La) has been reported to further reduce the creep rates[12,13] as well as to increase the real inline transmittance[4] in alumina. However, different atomistic mechanisms[9,14] have been proposed in the literature for the role of dopants in the sintering and strengthening effects and the issue is still far from settled.

Codoping can affect the properties of alumina by changing its microstructural features and/or transport mechanisms. Song and Coble[15] found that codoping with Mg in addition to Ca or Si gives an equiaxed structure in contrast to the platelike/abnormal grain structure when doped singly with Ca or Si. Song and Coble[16] also proposed a charge balance and strain balance condition for the appearance of platelike abnormal grains in codoped alumina. Swiatnicki et al.[17] reported that segregation of Mg to grain boundaries is suppressed when codoped with larger and higher charge cations like Ti, which was also supported by the ab initio simulation study of Elsässer and Elsässer.[18] Depletion of Mg was attributed to the "site competition" effect between Mg and the dopants or impurities of higher valence at grain boundaries.

Lartigue et al.[13] claimed that the constitutive laws change in high temperature deformation of alumina by Mg–Y codoping, i.e. yttrium segregates strongly to the grain boundaries and strengthens Mg doped alumina, which is more pronounced under tension than under compression. Gavrilov et al.[19] studied the

* Corresponding author at: MXC 210, EPFL-STI-IMX-LTP, Station 12, 1015 Lausanne, Switzerland. Tel.: +41 0 21 693 68 94; fax: +41 0 21 693 30 89.
E-mail address: abhishek.tewari@epfl.ch (A. Tewari).

0955-2219/$ – see front matter © 2012 Elsevier Ltd. All rights reserved.
doi:10.1016/j.jeurceramsoc.2012.02.056

Si–Mg codoped system and found that the grain boundary concentration of both ions is reduced by a factor of 5 or more over single doping. Additionally, codoping increases the mutual bulk solid solubility of the dopants, an effect which has also been studied by Dillon et al.[20] who used atomistic modeling, and by Elsässer and Elsässer[18] who did an ab initio study. The beneficial effect of MgO addition in controlling the microstructure of Si containing alumina was attributed to its ability to redistribute Si ions from the grain boundaries to the bulk.

Harmer and coworkers[12,21,22] conducted an extensive study to understand the beneficial effect of codoping on grain size in alumina and concluded it to be primarily a solid solution effect, as after precipitation, no further improvement with increasing dopant concentration was observed. They reported enhanced creep resistance in Nd–Zr codoped alumina compared to singly doped alumina due to cosegregation of both the dopants. It was postulated that different sized cations can produce a better packing at the interface and thereby reduce the free volume for grain boundary transport. Therefore, disparity of cation size was thought to be the main reason for additional effects of codoping on enhancing creep resistance. This logic was further strengthened by the findings of their simulation studies,[21] where they showed that doping with larger cations can break the mono-modal size distribution of cation substitutional sites volume and create several potential substitutional sites with varying sizes, many larger than the corresponding bulk sites. Therefore, dopants with different sizes can segregate easily to these sites and pack the interface efficiently. Elsässer and Elsässer[18] conducted several ab initio studies of codoping at the (0 0 0 1) grain boundary of alumina and reported that covalent dopant pairs prefer to arrange on nearest neighbor sites parallel to a rhombohedral plane, showing a coupling effect. They also reported that codoping of alumina with trivalent ions and bivalent/tetravalent ions can improve the covalent bonding for alumina since trivalent ions are accommodated chemically better than bivalent or tetravalent cations.

In the present study, we will focus on Y, La and Mg codoping. Since the bulk solubility of both Y and La is very low ($\leq$10 ppm) we assume that bulk interactions between the dopant only have minimal effect and we will therefore focus on surface and grain boundary structures. Ab initio studies being computationally expensive, only small systems with few 100 atoms can be calculated. Using classical atomistic modeling methods based on empirical potential provides an opportunity to consider larger systems as well as larger configurational space with lower computational cost. In our previous studies[23,24] it has been shown that satisfactory agreement between classical atomistic calculations and experimental as well as first principle results can be reached for alumina. The current simulation study aims to improve the understanding of the atomistic mechanisms behind doping and codoping using classical atomistic modeling methods. Energy minimization methods based on empirical potentials have been used to calculate relaxed surfaces and grain boundaries. The effect of doping and codoping has been studied on 9 surfaces and 8-grain boundaries for three codoping combinations: La–Y, La–Mg and Mg–Y. Segregation of dopants was observed to be energetically favorable in all the cases and a specific coordinative arrangement was observed in case of La–Y codoping. These results give interesting insights into interfacial energies and consequent grain growth for better control of microstructures toward transparent ceramics.

1.1. Computational method

The details of the computational method can be found in previous work.[23–26] Only relevant details of the method will be provided here. Doped and undoped equilibrium interface energies and structures were calculated using the Born model for solids, which has been implemented in METADISE.[27] The Born model describes interatomic forces in terms of pair potentials. A pair potential consists of an electrostatic potential and short range attractive as well as repulsive forces. In addition, the core–shell model by Dick and Overhauser[28] has been used to take into account the polarizability of oxygen ions. The potential parameters developed by Lewis and Catlow[29] were used in the present work and the initial alumina crystal structure has been taken from the work of Liu et al.[30] Nonpolar surface cuts were generated at different depths along the same surface normal and the lowest energy cut was chosen to create the final relaxed surface atomic structure. To create the mirror twin grain boundaries, two surfaces are put back to back allowing a rigid shift in the grain boundary plane. The minimum energy relative position of the two half crystals is chosen to create the final grain boundary structure. For surfaces as well as grain boundaries, 2D periodic boundaries are applied in the plane parallel to the interface. In the direction perpendicular to the interface, a two region model is applied where ions within ~9 Å from the interface are allowed to relax while the rest of the ions are kept fixed during energy minimization.[23,24] The bulk as well as the interface atomistic structures produced using the current method have been shown to be in good agreement with ab initio as well as experimental results.[23]

In order to reduce the otherwise large number of possible codoping configurations, energy minimization was performed only on what were estimated to be the highest probability configurations. First, interface Al ions within a certain distance of the interface (15 Å for La–Y codoping, 6 Å for Mg–La and Mg–Y codoping) were substituted one by one with the different dopants and the substitutional energy for each site was calculated for each dopant. The probabilities for a specific site were then calculated as follows: $[\exp(\Delta E_i)/\Sigma \exp(\Delta E_i)]$. ΔE_i is the energy of the site i (E_i) minus the energy of the farthest site from the interface. The probability of a specific multiple dopant configuration was then estimated as the product of the probabilities of each occupied site. For codoping, the probability of a particular codoping configuration is considered to be the product of respective single dopant configurations as illustrated in Fig. 1. For each dopant concentration, energy minimization was then done for the 150 configurations with the highest estimated probabilities.

In the case of the divalent dopant Mg, one oxygen vacancy has to be created for every two-dopant ions for charge neutrality. Our previous work on Mg doping showed that the Mg substitutional defect and oxygen vacancies are not coupled and

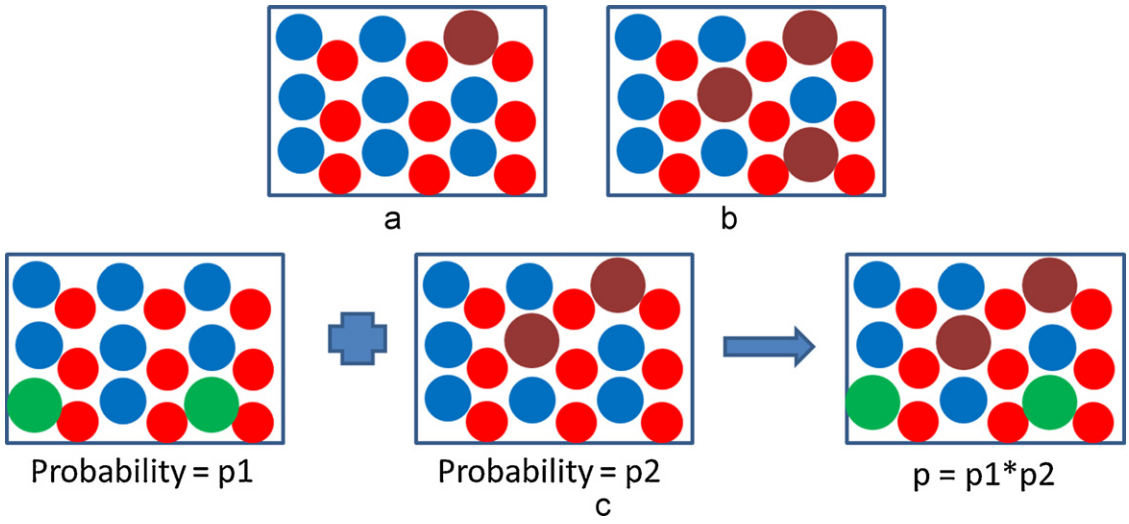

Fig. 1. (a) single site substitution, (b) permutation of lowest energy sites for multiple dopant configurations, (c) codoping configuration as a combination of respective single dopant configurations.

therefore should be treated independently.[24] Consequently the substitutional Mg defect and oxygen vacancy defect (V_O) were considered separately in the present work instead of considering a cluster defect of Mg–V_O–Mg. Therefore, the bulk defect energies of substitutional Mg and oxygen vacancies are subtracted separately in the expression (Eq. (2)) for segregation energy calculation. For a pair of Mg dopants, there are a large number of possible oxygen vacancy positions. In order to address this problem, the interface width was divided in slabs of widths of 2 Å. For a certain pair of divalent dopant ions in a slab, oxygen vacancies were created only in the same slab. Thereafter, the probabilities for Mg sites as well as vacancy sites were calculated in a similar fashion as for trivalent dopants. The lowest energy Mg sites and vacancy sites were permutated in order to get the lowest energy configurations of multiple Mg doped alumina interfaces.

In order to check the accuracy of the configuration probability estimation, energy minimization was also performed on 1000 and 1500 randomly chosen configurations for trivalent and bivalent dopants, respectively. The results show that the minimum energy configurations are always obtained by the doping strategy employed in the present case, while the energy of the random configurations was always higher as shown by examples in Fig. 2.

The segregation energy of the codoping was calculated using the expression:

$$\Delta H_{seg}(N_Y + N_{La}) = \frac{(H(N_Y + N_{La}) - H(0) - N_Y \Delta H_{Y,bulk} - N_{La}\Delta H_{La,bulk})}{(N_Y + N_{La})} \quad (1)$$

Table 1
Sigma values of the twin grain boundaries, surface area (A) of the cells used for the calculations and interfacial energies of grain boundaries (γ_{GB}) and surfaces (γ_{surf}) calculated in the present work. Sigma values is the ratio of the lattice points in the unit cell of coincident site lattice and the original lattice.

Miller indices	Σ	γ_{surf} (J/m^2)	γ_{GB} (J/m^2)	A (nm^2)
(00.1)	3	2.99	2.66	0.7713
(01.2)	7	2.62	0.27	0.7020
(10.0)	3	2.89	0.5	0.5866
(11.2)	7	3.44	2.85	1.0867
(10.1)	11	3.67	1.88	0.6175
(11.0)	–	3.02	–	1.0160
(11.3)	13	3.20	2.42	1.1691
(22.3)	43	3.18	2.95	2.1127
(11.1)	93	3.48	2.87	1.0341

$\Delta H_{seg}(N)$ is the enthalpy of segregation in a structure containing N dopant ions, $H(N)$ is the potential energy of the structure containing N dopant ions, and $\Delta H_{i,bulk}$ is the change in enthalpy when inserting a dopant ion i or oxygen vacancy in the bulk. For Y–La codoping, 9 surfaces and 8-grain boundaries were considered. All the grain boundaries were mirror twin grain boundaries of the same indices as the surfaces. (1 1 0) surface is parallel to a mirror plane of the crystal and therefore a (1 1 0) mirror twin grain boundary is equivalent to the bulk alumina. For Mg–La and Mg–Y codoping, 5 surfaces and the corresponding 4 mirror twin grain boundaries were studied. A brief summary of the grain boundaries and surfaces calculated in the present work is given in Table 1. Additionally, since it was impossible to explore all possible combinations of dopant concentrations, we restricted ourselves to the case of equal dopant concentration for both dopants.

$$\Delta H_{seg}(N_{Mg} + N_{La}) = \frac{1}{(N_{Mg} + N_{La})}\left(H(N_{Mg} + N_{La}) - H(0) - N_{La}\Delta H_{La,bulk} - N_{Mg}\Delta H_{Mg,bulk} - \frac{N_{Mg}}{2}\Delta H_{Ovac,bulk}\right) \quad (2)$$

In order to characterize the atomic arrangement at the interface a coordination number (CN) was determined by counting the number of atoms within a cut off radius. Cut off radii were taken[11,31] as Y–O: 2.9 Å, La–O: 3.1 Å, Mg–O: 2.7 Å, Y–Y: 4.54 Å, Y–La: 4.65 Å, La–La: 4.76 Å. Cut off radii were determined as the center of the nearest neighbor and second neighbor distance where the coordination number remains constant for a certain range of cut off radius.

1.2. Theoretical considerations

Whereas the case of single doping has been studied quite extensively and an expression for the ratio between the interface (X^i) and bulk cationic ratio (X^b) in function of the segregation energy (ΔH_{seg}) has been developed by Mackrodt and Tasker,[32] the case of codoping has, to our knowledge, not been looked at thoroughly from a theoretical standpoint. However an expression for X^i/X^b very similar to the case of single doping can be derived analogically to the Mackrodt and Tasker derivation for single doping (see Supplementary material).

$$X^i_{D1} = X^b_{D1} \cdot e^{-((\Delta H^{D1}_{seg}(X^i_{D1},X^i_{D2})+X^i_{D1}(X^i_{D1}+1)(\partial \Delta H^{D1}_{seg})/(\partial X^i_{D1})+X^i_{D2}(X^i_{D1}+1)(\partial \Delta H^{D2}_{seg}/\partial X^i_{D1}))/(kT))} \quad (3)$$

The subscripts D1 indicate one dopant and D2 the other, k is the Boltzmann constant and T the temperature. The biggest difference to the case of single doped segregation is that the expression is now also dependent on the change of the segregation energy of the second dopant with respect to the dopant concentration of the first.

Since we restricted ourselves to equal interfacial dopant concentrations in this work we can set $X^i_{D,tot} = X^i_{D1} + X^i_{D2}$ and $X^i_{D1} = X^i_{D2} = 0.5 * X^i_{D,tot}$. If additionally we consider the case where codoping is neither energetically favorable nor disfavorable and hence the segregation energy of a dopant is only dependent on the total dopant ionic ratio ($X^i_{D,tot}$) at the interface and not on the individual ratios of each dopant (X^i_{D1} and X^i_{D2}) we can simplify Eqs. (3) and (4).

$$0.5 \cdot X^i_{D,tot} = X^b_{D1} \cdot e^{-(\Delta H^{D1}_{seg}(X^i_{D,tot})+0.5\cdot X^i_{D,tot}(0.5X^i_{D,tot}+1)(\partial \Delta H^{D1}_{seg}/\partial X^i_{D,tot})+0.5\cdot X^i_{D,tot}(0.5\cdot X^i_{D,tot}+1)(\partial \Delta H^{D2}_{seg}/\partial X^i_{D,tot}))/(kT)} \quad (4)$$

For the sake of discussion let us suppose that the shape of the ΔH_{seg} vs. X^i curves for the different dopants are very similar and hence the derivative of both ΔH^{D1}_{seg} and ΔH^{D2}_{seg} with the total dopant concentration to be about equal. According to our results, this assumption is not too far off (see Fig. 3).

$$0.5 \cdot X^i_{D,tot}(0.5X^i_{D,tot}+1)\frac{\partial \Delta H^{D1}_{seg}}{\partial X^i_{D,tot}} + 0.5 \cdot X^i_{D,tot}(0.5 \cdot X^i_{D,tot}+1)\frac{\partial \Delta H^{D2}_{seg}}{\partial X^i_{D,tot}} \approx X^i_{D,tot}(X^i_{D,tot}+1) \times \frac{\partial \Delta H^{D1}_{seg}}{\partial X^i_{D,tot}} \quad (5)$$

With this assumption we can see that the derived expression (Eq. (4)) is very similar to the case of single doping (Eq. (6)), see Mackrodt and Tasker[32] for more details) except for the factor of 0.5 in front of the interfacial dopant concentration. This means that at the same bulk concentration of dopant one X^b_{D1} we have a higher total interfacial dopant concentration $X^i_{D,tot}$. This again means that, if we assume there are no interactions between the dopants in the bulk because of their low concentration (≤10 ppm for La and Y) and hence the bulk solubility of both dopants being the same in the case of single doping and codoping, we have a higher total interfacial dopant concentration at the solubility limit in the case of codoping than in the case of single doping. The reason for this is the additional configurational entropy of having two instead of only one dopant (see Supplementary material).

$$X^i_{D,tot} = X^b_{D1} \cdot e^{-(\Delta H^{D1}_{seg}(X^i_{D,tot})+X^i_{D,tot}(X^i_{D,tot}+1)(\partial \Delta H^{D1}_{seg}/\partial X^i_{D,tot}))/(kT)} \quad (6)$$

For the case discussed above (i.e. neither favorable nor disfavourable interactions between D1 and D2) we should observe a codoping segregation energy ΔH_{seg} which is the average of the segregation energies of D1 and D2 (i.e. $\Delta H_{seg} = 0.5 * \Delta H^{D1}_{seg} + 0.5 * \Delta H^{D2}_{seg}$), if there is no favorable interaction between different type of dopants. In the following discussion we will hence consider any calculated ΔH_{seg} below $0.5 * \Delta H^{D1}_{seg} + 0.5 * \Delta H^{D2}_{seg}$ to be indicative of favorable interactions between the dopants of different types. Any ΔH_{seg} above that value would indicate disfavourable interactions such as e.g. site competition between D1 and D2.

2. Results and discussion

2.1. Segregation energies

2.1.1. La–Y codoping

Nine surfaces and 8 grain boundaries were calculated for Y–La codoping. For all dopant concentrations, single doped and codoped, the segregation energies are negative as listed in Table 2. Therefore, segregation to the surfaces and grain boundaries is energetically favorable for all systems studied. Segregation energy for La–Y codoping varies from −2.14 to −5.25 eV/atom for surfaces and from −1.57 to −4.27 eV/atom for different grain boundaries, which indicates stronger segregation on surfaces than GB's. It should be noted that the segregation energies calculated for Y in the present work are slightly more negative (0.5–1.0 eV/atom) in comparison to the

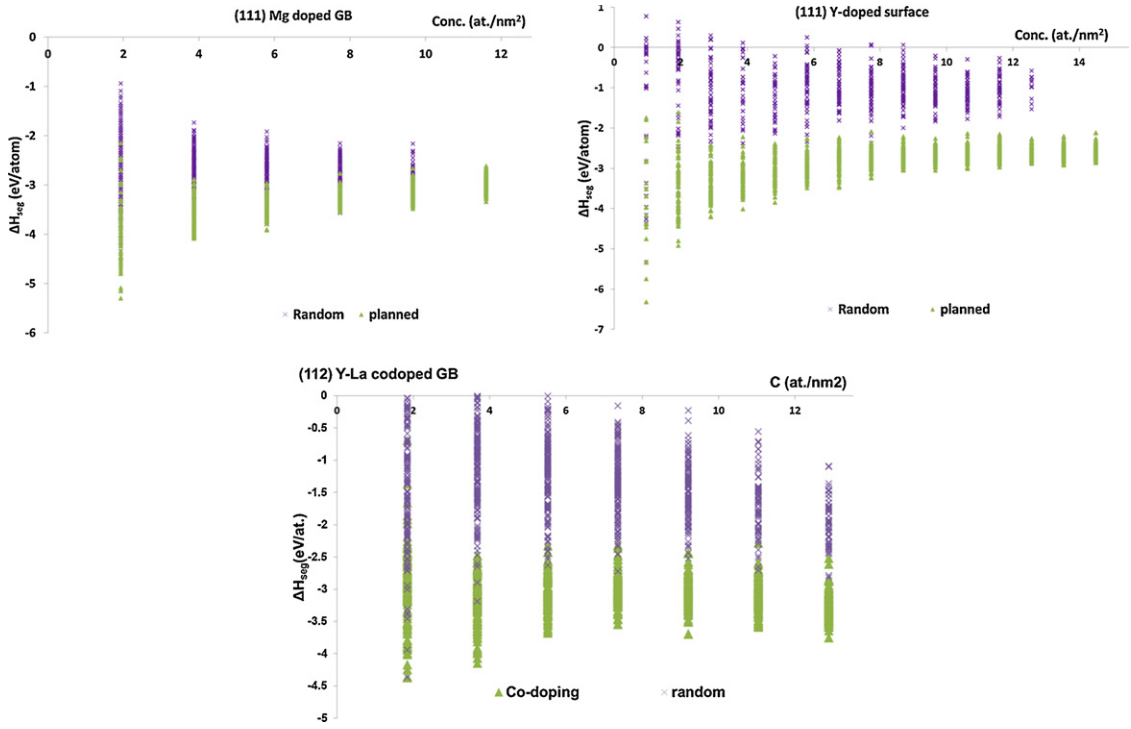

Fig. 2. Comparison of probabilistic codoping with randomly chosen configurations.

energies calculated in our previous work[23] due to the more efficient method of selecting low energy configurations, especially at higher dopant concentrations. However the general behavior, i.e. often observed important energy minima, does not change. It may lead to higher solubility of dopants at interfaces than we calculated earlier.[24]

Codoping segregation energy for La–Y codoped surfaces increases continuously for low concentrations and reaches a constant value of −2.14 to −5.25 eV at a dopant concentration of about ∼8–10 atoms/nm^2 (Fig. 3a). Analysis of the simulated atomistic structures shows that 8–10 atoms/nm^2 is the dopant concentration which is required for the complete coverage of the surface Al sites with dopants and Al surface sites are no longer available to be substituted by the dopants. As the interface Al sites are filled up, the sites that remain available become energetically less favorable and hence the asymptotic value of segregation energy is reached after this concentration.

In the case of Y–La codoped grain boundaries, segregation energy for codoping neither decreases nor increases for (00.1) GB. For other low Σ grain boundaries, ((01.2), (10.0), and (10.1)), segregation energy decreases with concentration (Fig. 3b). A minimum is observed for (01.2) GB at 7–8 atoms/nm^2 dopant concentration and a change in the slope is observed for (10.0) GB around the same concentration. For the higher Σ surfaces (i.e. (11.1), (11.2), (11.3), and (22.3)), the segregation energy for codoping increases with dopant concentration and approaches a constant value from 6–8 atoms/nm^2 similar to the surfaces (Fig. 3b). This concentration is similar to the concentration corresponding to minima observed in the case of low index grain boundaries (6–8 at./nm^2). One possible explanation for the decreasing segregation energy with increasing concentration in the case of low index grain boundaries might be that pure interfaces are closely packed and therefore cannot accommodate larger size cations. In the beginning as the dopant concentration increases, atomic rearrangement takes place at the interface, which leads to more open interface structures favoring segregation. After a critical concentration, atomic rearrangement no longer remains energetically favorable, since the GB is saturated and hence the segregation energy remains constant.

To compare segregation energies of codoped interfaces with single doping, a curve corresponding to [$\Delta H_{seg,\,min}$(D1,C)

Table 2
Asymptotic/local minimum segregation energy values (ΔH_{seg}) and corresponding concentration (C) for La–Y codoped surfaces and grain boundaries.

	C_{surf} (at./nm^2)	$\Delta H_{seg,\,surf}$ (eV)	C_{gb} (at./nm^2)	$\Delta H_{seg,\,gb}$ (eV)
(00.1)	10.3720[a]	−5.25[a]	5.1860[b]	−3.84[b]
			10.372[b]	−4.07[b]
(01.2)	14.2453[b]	−4.15[b]	8.5472[b]	−2.9[b]
(10.0)	10.2291[a]	−4.61[a]	6.8194[d]	−1.57[d]
			10.2291[d]	−2.34[d]
(10.1)	9.7174[a]	−2.14[a]	6.4783[b]	−2.98[b]
			16.1957[b]	−3.44[b]
(11.0)	9.8429[a]	−4.06[a]	–	–
(11.1)	9.6703[a]	−4.41[a]	7.7362[a]	−4.27[a]
(11.2)	9.2022[a]	−4.38[a]	7.3618[a]	−3.55[a]
(11.3)	8.5535[a]	−4.54[a]	6.8428[a]	−3.9[a]
(22.3)[c]	6.6267	−4.23	6.6267	−3.16

[a] Asymptotic ΔH_{seg} and C.
[b] Value of ΔH_{seg} and C at a local minima.
[c] Neither asymptotic value nor minimum is observed.
[d] change in the slope of the energy curve.

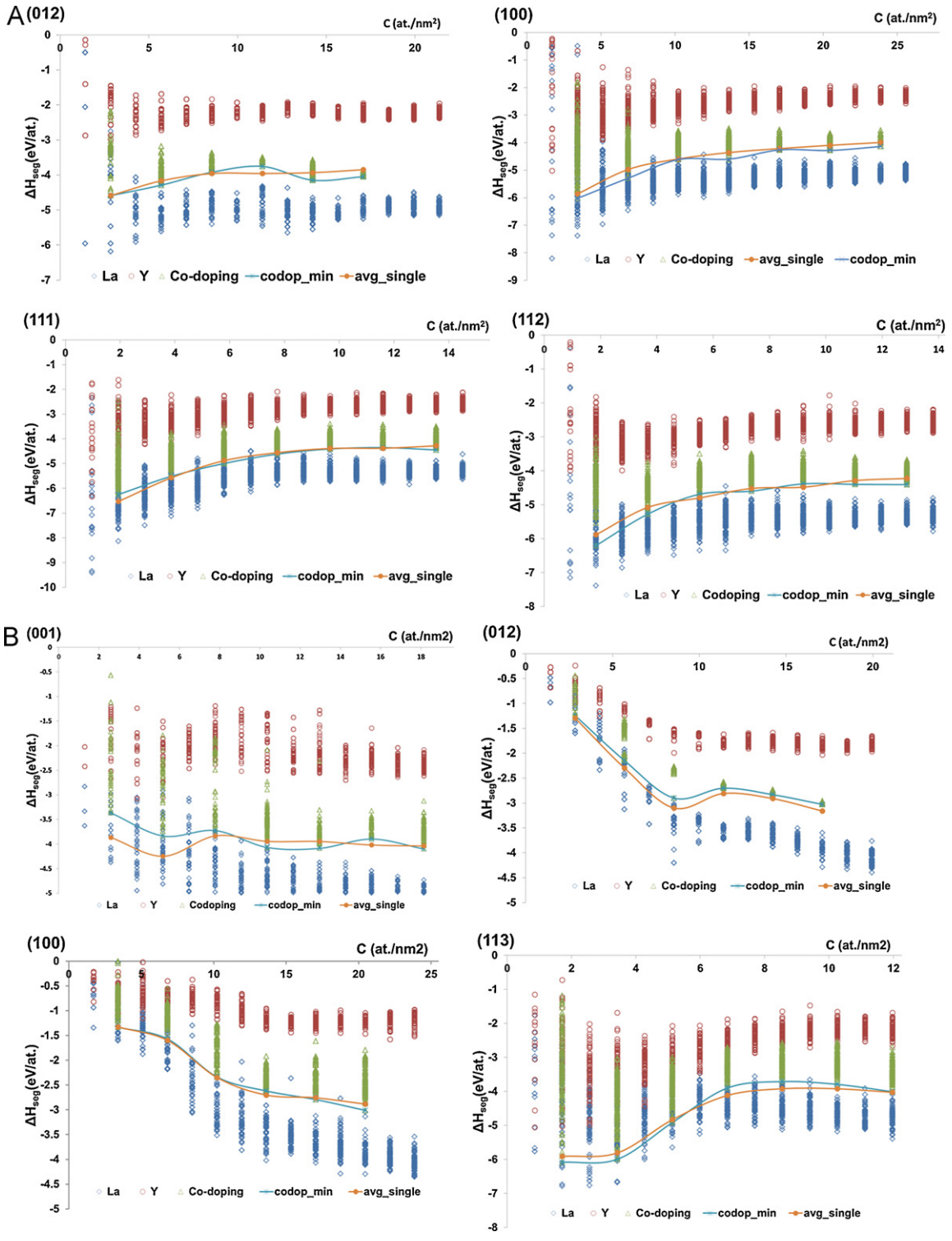

Fig. 3. Representative segregation energy plots for La–Y codoped (a) surfaces, and (b) GB's. The lines serve as visual guides only.

$+ \Delta H_{\text{seg, min}}(\text{D2,C})]/2$ is shown in the segregation energy plots, where $\Delta H_{\text{seg, min}}(\text{D1,C})$ is the minimum segregation energy of singly doped interface at a concentration C of dopant D1. As discussed in Section 2.2, the codoped configurations, which have segregation energy below this curve, are energetically more favorable than single doping. Only (10.0) and (22.3) surfaces have slight energetic gain over single doping. For grain boundaries energetically favorable interactions have only been observed for the (01.2) grain boundary possibly due to the specific ordering of the dopants on this specific grain boundary that will be discussed further in the next section. All other Y–La codoped surfaces and grain boundaries have no clear energetic gain/loss over single doping as shown through some representative segregation energy plots in Fig. 3. In general, therefore there

Table 3
Segregation energy values (ΔH_{seg}) and corresponding concentration (C_1 and C_2) for Mg–La Codoped surfaces and grain boundaries. C_1 and C_2 are the interface dopant concentrations when 4 and 8 dopant atoms are put on the interface respectively.

	C_1 (at./nm^2)	$\Delta H_{seg,surf}$ (eV)	$\Delta H_{seg,GB}$ (eV)	C_2 (at./nm^2)	$\Delta H_{seg,surf}$ (eV)	$\Delta H_{seg,GB}$ (eV)
(00.1)	5.186	−6.44	−4.65	10.372	−5.47	−4.14
(01.2)	5.6981	−4.33	−2.14	11.3962	−4.25	−2.69
(11.0)	7.8743	−4.49		11.8115	−4.25	
(11.1)	7.7362	−4.91	−4.52	11.6043	−4.49	−4.16
(11.3)	6.8428	−4.57	−4.63	10.2642	−4.69	−4.27

is no conclusive favorable/unfavorable interaction between La and Y dopant ions at codoped interfaces.

Another important point to be noted is that the codoping segregation energies for different configurations with the same concentration have a much more continuous spectrum, no particularly lowest energy configurations are observed contrary to the single doping cases (Fig. 3). This will lead to an increase in the configurational entropy for segregation in case of codoping due to higher number of comparable energy configurations.

2.1.2. *Mg–La codoping*

Calculations were done for 5 surfaces and 4 grain boundaries for Mg–La and Mg–Y codoping. In case of codoping with Mg as one of the dopants, the concentrations which can be calculated are restricted due to the fact that one O vacancy has to be included for 2 Mg ions in the structure. Therefore concentrations are more discrete in comparison to Y–La case and hence it is difficult to comment on the pattern of the codoping segregation energy variation with dopant concentration in this case. Segregation energies for codoping are again negative for all the interfaces as shown in Table 3. Again, the Mg segregation energy calculated in the present work is 0.5–1.0 eV lower than reported in our earlier work[24] due to improved method to choose lowest energy configurations. It may increase the solubility of the dopants at the interfaces and hence the previously calculated[24] overall nominal solubility as well.

Fig. 4 shows some representative segregation energy plots of Mg–La codoped surfaces and grain boundaries. Codoping segregation energy increases for all the Mg–La codoped grain boundaries except for (01.2), where it decreases with increasing dopant concentration (Fig. 4(b) left panel). The segregation energy is always more negative for surfaces than GB's suggesting stronger segregation toward surfaces than GB's in this case as well.

Segregation is energetically more favorable for all the Mg–La codoped surfaces and grain boundaries except for (01.2) grain boundary in comparison to single doping, as codoping segregation energy plots lie below the average of the single doping segregation energy plots (Fig. 4). It suggests that there is favorable interaction between segregated Mg and La dopants on interfaces, which may be attributed to the presence of oxygen vacancies in this case. Due to the creation of oxygen vacancies

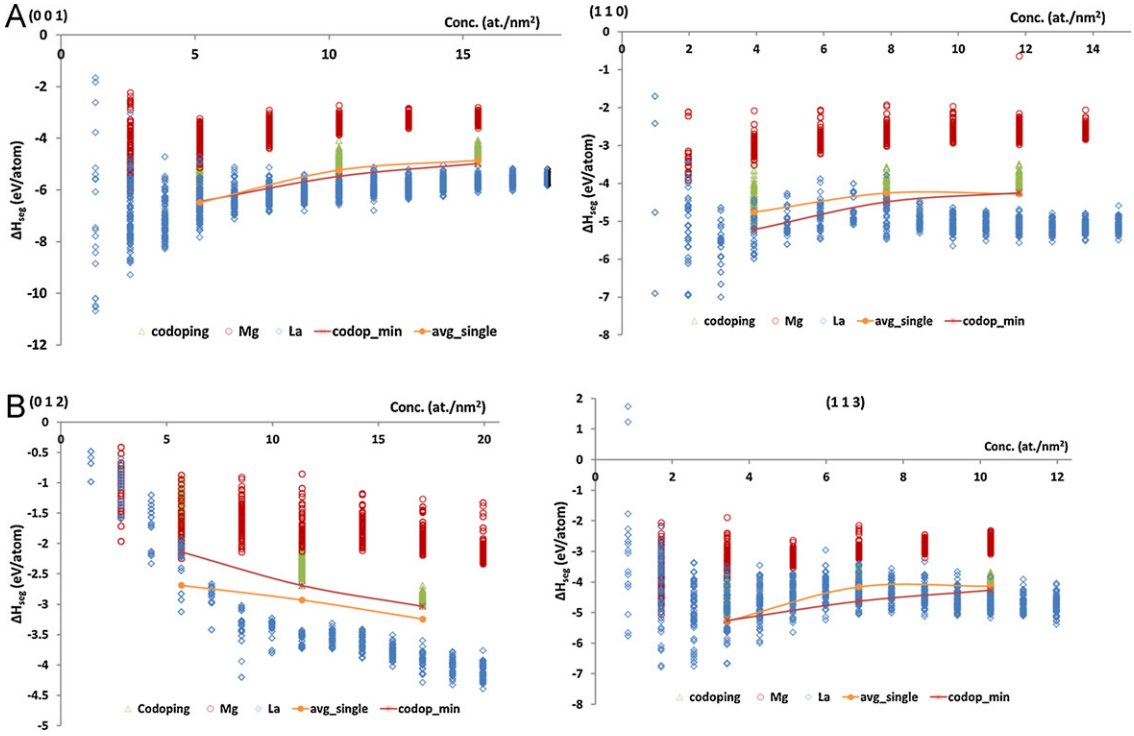

Fig. 4. Representative segregation energy plots for Mg–La codoped (a) surfaces and (b) GB's. The lines are visual guides only.

Table 4
Segregation energy values (ΔH_{seg}) and corresponding concentration (C_1 and C_2) for Mg–Y codoped surfaces and grain boundaries. C_1 and C_2 are the interface dopant concentrations when 4 and 8 dopant atoms are put on the interface respectively.

	C_1 (at./nm^2)	$\Delta H_{seg,surf}$ (eV)	$\Delta H_{seg,GB}$ (eV)	C_2 (at./nm^2)	$\Delta H_{seg,GB}$ (eV)	$\Delta H_{seg,GB}$ (eV)
(00.1)	5.186	−5.04	−2.95	10.372	−4.14	−3.94
(01.2)	5.6981	−2.14	−2.84	11.3962	−2.69	−2.68
(11.0)	7.8743	−3.02				
(11.1)	7.7362	−3.4	−3.6	11.6043	−3.15	−3.18
(11.3)	6.8428	−3.06	−3.62	10.2642	−3.1	−3.2

there is more free space available for the segregation of larger size dopants and it acts as driving force for segregation. The specific atomic ordering of the dopants is observed on (01.2) grain boundary similar to the La–Y case.

2.1.3. Mg–Y codoping

Similar to other codoping combinations, the segregation energy for single as well as codoping is negative for all the interfaces. Again segregation toward surfaces for Y–Mg codoping is energetically more favorable than toward grain boundaries (Table 4). The cosegregation energy increases with increasing dopant concentration for all calculated surfaces and grain boundaries except for (01.2) GB, where it decreases with increasing concentration as shown in Fig. 5.

Except (11.3) surface and (01.2) grain boundary, segregation is energetically more favorable for calculated Mg–Y codoped surfaces and grain boundaries than single doping average as shown in Fig. 5, and hence there is favorable interaction between Mg and Y dopants on the interfaces. As mentioned earlier the favorable interaction in this case might be attributed to the additional driving force due to more available space created by the oxygen vacancies.

2.1.4. Results: summary

For grain boundaries the segregation energies (Tables 2–4) for the low energy grain boundaries (01.2) and (10.0) are less negative (La–Y: 1.57–2.9 eV; Mg–La: 2.69 eV; Mg–Y: 2.68 eV) than for the other grain boundaries (La–Y: 2.98–4.27 eV; Mg–La: 4.14–4.27 eV; Mg–Y: 3.18–3.94 eV). This leads to the homogenization of the grain boundary energies and hence to the homogenization of the sintered microstructure and a lower percentage of highly special low Σ twin boundaries. This has also been reported in case of Mg doping in our earlier study.[24] However even in undoped alumina the percentage of low energy Σ twin boundaries is very low[33] and a change in the homogeneity of the microstructure upon doping is not observed.[4,33] For surfaces the segregation to low and high-energy surfaces are similar. The segregation energies for the (00.1) surface is significantly more negative than for the other surfaces in all the codoped cases (Tables 2–4). Since the (00.1) surface is one of the lowest energy surfaces the highly negative segregation energies

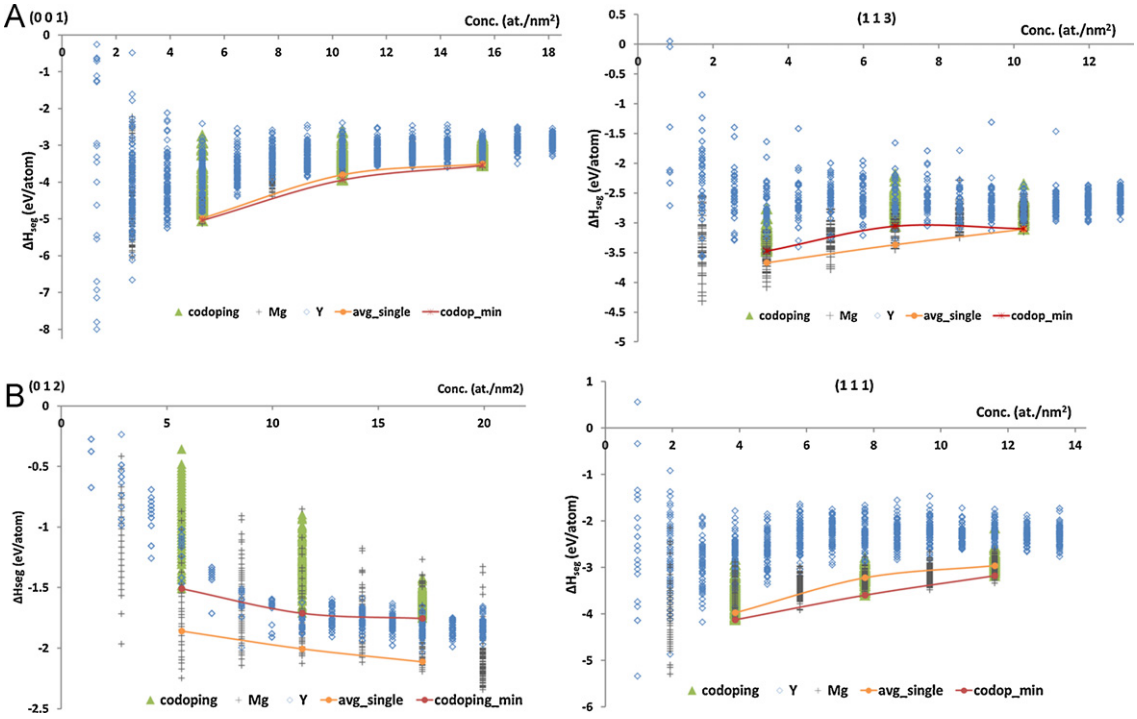

Fig. 5. Representative segregation energy plots for Mg–Y codoped (a) surfaces and (b) GB's. The lines are visual guides only.

might be supposed to lead to a very low relative (00.1) surface energy and hence the domination of equilibrium morphology by the (00.1) surface (i.e. platelet like morphology).

Segregation energy calculations show that while Mg–La and Mg–Y codoping combinations are energetically more favorable in comparison to single doping, La–Y codoping does not have any significant energetic gain over single doping. Two factors are likely to contribute to the favorable Mg–Y and Mg–La interactions. The first factor is the creation of oxygen vacancies to compensate the charge of the Mg dopants on the Al sites. The presence of oxygen vacancies can be supposed to create more space for the accommodation of the significantly oversized Y and La ions. If the presence of oxygen vacancies is responsible for the energetic gain, sintering in vacuum should increase the amount of Y and/or La dopants at the interfaces similar to the addition of Mg because it increases the concentration of oxygen vacancies.

The second factor is the disparity in ionic sizes of the dopants (Mg^{2+}: 0.86 Å, Y^{3+}: 1.04 Å, La^{3+}: 1.17 Å). Harmer et al.[21] showed in their atomistic simulation work that doping with larger cations can break the unimodal size distribution and create several potential substitutional sites with varying sizes, many larger than the corresponding bulk sites. These sites can probably easily accommodate the Mg ions, which are relatively smaller to other dopants. If this is the main reason for the energy gain, codoping of La or Y with an isovalent dopant with smaller radius (e.g. Indium (0.94 Å) should also be energetically favorable.

Comparison of the codoping segregation energies for different codopant combinations shows that the segregation energy is most negative for Mg–La dopant pairs (i.e. $\Delta H_{seg,Mg-La} \leq \Delta H_{seg,Y-La} < \Delta H_{seg,Mg-Y}$) for all the calculated surfaces and grain boundaries, as shown in Fig. 6. The difference between Mg–La and Y–La segregation energy is not very marked, while the cosegregation energy for Mg–Y is significantly higher. This order is consistent with the order of segregation energies for single doped (i.e. $\Delta H_{seg,La} < \Delta H_{seg,Mg} \leq \Delta H_{seg,Y}$). The observed interaction energies as discussed in the previous sections do not alter the energetic order of the segregation energies. This is not surprising as in most cases the observed interaction energies between the different dopants were small.

2.2. Interface atomic structure characteristics

Atomistic structures of the codoped surfaces and grain boundaries show that the dopants are confined to a very narrow region at the interfaces for all the dopant combinations and all the interfaces. Fig. 7 shows illustrative atomistic structures of Y–La codoped surfaces and grain boundaries at characteristic interface dopant concentrations as mentioned in Table 2 in the previous section. Observation of the atomistic structures suggests that segregation is sensitive to surface and grain boundary structure as suggested in the recent work where such specific structure dependence has been termed complexion.[34] That is to say clear differences can be seen in the atomic arrangement of dopants between for instance the (01.2) and (11.3) surface as well as the grain boundaries. While dopants form an ordered atomic layer at the (01.2) interfaces, they are randomly distributed at the (11.3) interfaces.

The dependence on the underlying interface structure can also be seen when looking at the packing efficiency. Dopants affect the packing efficiency of surfaces and grain boundaries differently depending on the interface and the dopant combination. The same dopants may improve the atomic packing at some of the interfaces but create more spaces/voids on other interfaces. To confirm the effect of dopants on atomic arrangement of the interfaces, packing fractions were calculated for single doped and codoped grain boundaries. Packing fractions were determined by calculating the ratio of occupied volume of the grain boundary region (according to the ionic radii of the different ions) to the total volume of the considered grain boundary region. The average packing fraction was determined from all the calculated codoping configurations at different doping concentrations. The calculated packing fraction values (Table 5) show that the packing fractions vary quite significantly depending on the nature of the grain boundary as well as the doping combinations. Y doped grain boundaries are denser in comparison to La doped or La–Y codoped grain boundaries. Similarly, Mg doped grain boundaries have higher packing efficiency than La doped or Mg–La codoped grain boundaries. However, in case of Mg–Y codoping, no conclusion can be drawn regarding effect of codoping on grain boundary packing efficiency since packing efficiency increases in few cases and decreases in others, depending on the grain boundaries.

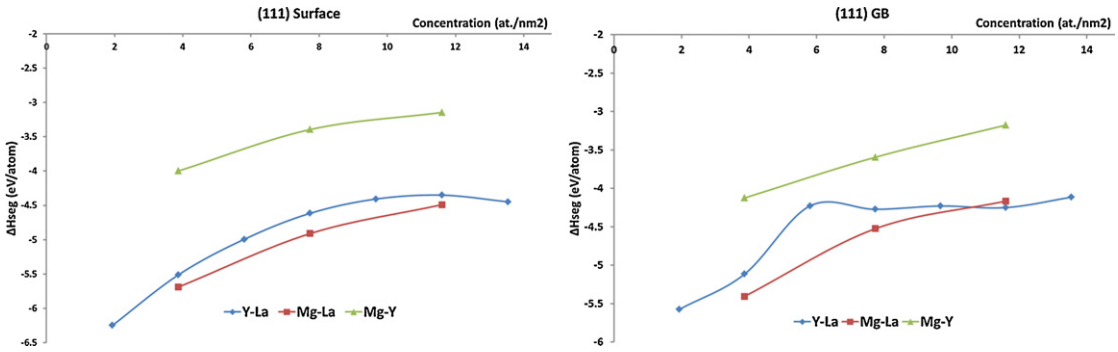

Fig. 6. Codoping segregation energy comparison for three doping combinations. The lines are visual guides only.

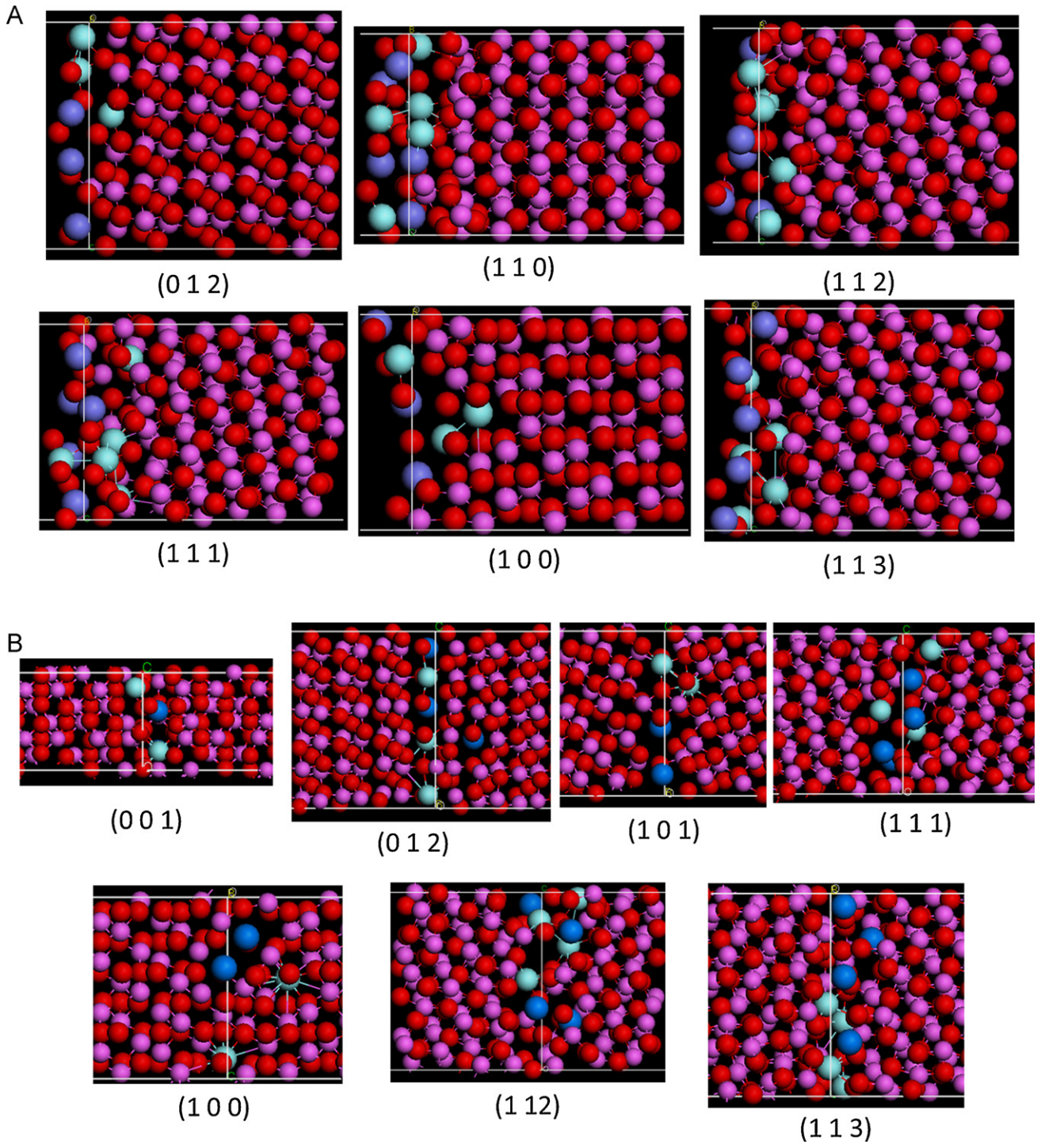

Fig. 7. Interface structure dependent cosegregation and atomic arrangment of La–Y codoped α-alumina (a) surfaces and (b) grain boundaries. All the atomistic structures are shown from the side view parallel to the grain boundary/surface plane with the white lines showing roughly the position of the grain boundary or surface plane. Oxygen ions are shown in red, aluminum ions in violet, Y in light blue and La in dark blue. (For interpretation of the references to color in this figure legend, the reader is referred to the web version of the article.)

There is no specific pattern formation by the dopants at the codoped grain boundaries, with the exception of the (01.2) grain boundary where a pattern is observed for all three codoping combinations. As shown in Fig. 8 dopants occupy positions which form an atomic layer parallel to the grain boundary. Dopants first exhaust the interface Al sites available before going to the next sub-surface layers leaving on original alumina atomic layer intact in between. The absence of pattern formation for the majority of interfaces studied is in contrast to the formation of geometric patterns by Y in many of the single doped alumina surfaces and grain boundaries at minimum energy concentrations, observed in earlier simulation studies.[23] This is also consistent

Table 5
Packing fractions of the single and codoped grain boundaries (grain boundary width for packing fraction calculation was taken 10 Å for La–Y, La and Y doping, while 6 Å for Mg–Y, Mg–La and Mg doped, 6 Å for undoped grain boundaries).

	La	Y	Mg	La–Y	Mg–La	Mg–Y	Undoped
(00.1)	0.59	0.64	0.65	0.63	0.63	0.69	0.68
(01.2)	0.59	0.62	0.58	0.62	0.56	0.58	0.62
(10.0)	0.53	0.61	–	0.57	–	–	0.63
(10.1)	0.53	0.61	–	0.57	–	–	0.64
(11.1)	0.55	0.58	0.57	0.56	0.58	0.59	0.58
(11.2)	0.57	0.60	–	0.58	–	–	0.62
(11.3)	0.58	0.62	0.64	0.60	0.59	0.63	0.68
(22.3)	0.61	0.61	–	0.61	–	–	0.58

with the fact that in general upon codoping no minimal energy configuration is observed, the energies calculated for the different configurations for a specific dopant concentration seem to form a continuous energy band, indicating a higher configurational entropy in the case of codoped than in the case of single doped interfaces.

In general codoping is observed to produce more ordered and packed atomistic structures at the interfaces. This effect is most pronounced when La doped structures are compared to Mg–La and Y–La codoped structures, due to its higher size mismatch. For example, as shown in Fig. 9, in comparison to La-doped (11.1) grain boundary (Fig. 9b), Mg–La and Y–La codoped grain boundaries (Fig. 9d and f) have more ordered and rigid structure. The effect is also visible for Mg and Y dopants, but to a lesser extent.

2.3. Coupling effect

As mentioned in the previous section, there is no energetic gain for cosegregation over single dopant segregation in case of Y–La codoped surfaces and grain boundaries. However, an atomistically preferred arrangement of the dopants is observed in the case of Y–La codoping. As shown in Fig. 10, dopants of different species arrange themselves around the oxygen at nearest neighbor positions. An oxygen ion seems to be more often coordinated by an Y and a La than by two La or two Y. To confirm the atomistic observations coordination numbers (CN) were determined for different surfaces and grain boundaries from the atomistic structures of the interfaces at characteristic concentrations for each interface as mentioned in Table 2. Coordination number for Y–La was found to be higher in comparison to Y–Y and La–La coordination numbers for all the surfaces and grain boundaries, (10.1) and (11.1) grain boundaries being the only exceptions. CN's for both Y–Y (2.39) and La–La (3.55) are higher than Y–La (2.17) for (10.1) grain boundary. Similarly, for (11.1) grain boundary La–La CN (2.39) is higher than Y–La CN (2.09). For other grain boundaries, the coordination number for Y–La varies from 1.53 to 2.22, while for Y–Y and La–La it varies from 0.51 to 1.64 and 0.83 to 1.43, respectively. Similarly the coordination number of Y–La, Y–Y and La–La varies from 1.81 to 3.01, 1.39 to 2.2 and 0.98 to 1.94, respectively for codoped surfaces. Higher coordination number for Y–La in comparison to Y–Y and La–La for each individual interface shows the higher probability of Y and La at nearest neighbor position around oxygen. In an ab initio study, Elsässer and Elsässer[18] also observed a similar specific atomic arrangement of dopants on rhombohedral twin boundary of alumina when codoped with bivalent/trivalent dopant ions. They reported that in case of codoping, dopant pairs prefer to arrange on nearest neighbor sites parallel to rhombohedral plane, showing a coupling effect.

2.4. Dopant–oxygen coordination number

The dopant–oxygen coordination numbers (CN) have been calculated for all the codoping cases. The characteristic concentrations to calculate dopant–oxygen coordination number for La–Y codoping were taken from Table 2. For Mg–Y and Mg–La codoping the concentration corresponding to 8 dopant ions was considered to calculate the dopant–O CN. In accordance with the different geometry (i.e. at the surface neighbors normally found in the bulk are missing whereas at grain boundaries only their relative positions will change), coordination numbers are higher for grain boundaries than for surfaces. The dopant–oxygen coordination numbers do not vary much from one codoping combination to another (Table 6). No significant change in Y–O and Mg–O coordination environment between

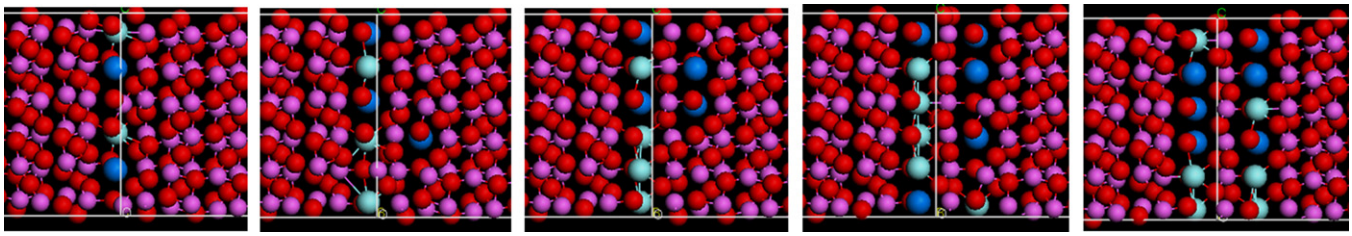

Fig. 8. Formation of dopant atomic layer on Y–La codoped (01.2) grain boundary with increasing dopant concentration. Oxygen ions are shown in red, aluminum ions in violet, Y in light blue and La in dark blue. (For interpretation of the references to color in this figure legend, the reader is referred to the web version of the article.)

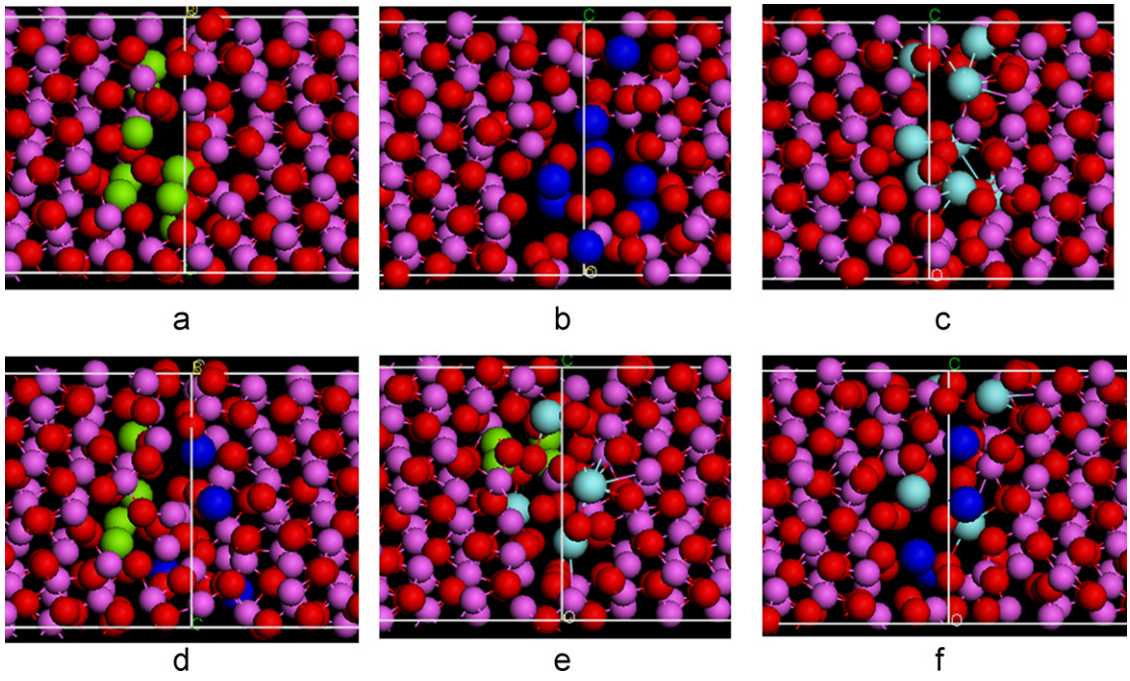

Fig. 9. Comparison of single doped and codoped (11.1) grain boundaries (a) Mg doped, (b) La-doped, (c) Y-doped, (d) Mg–La codoped, (e) Mg–Y codoped, and (f) La–Y codoped (concentration = 7.74 at./nm^2). Oxygen ions are shown in red, aluminum ions in violet, Y in light blue, La in dark blue and Mg in green. (For interpretation of the references to color in this figure legend, the reader is referred to the web version of the article.)

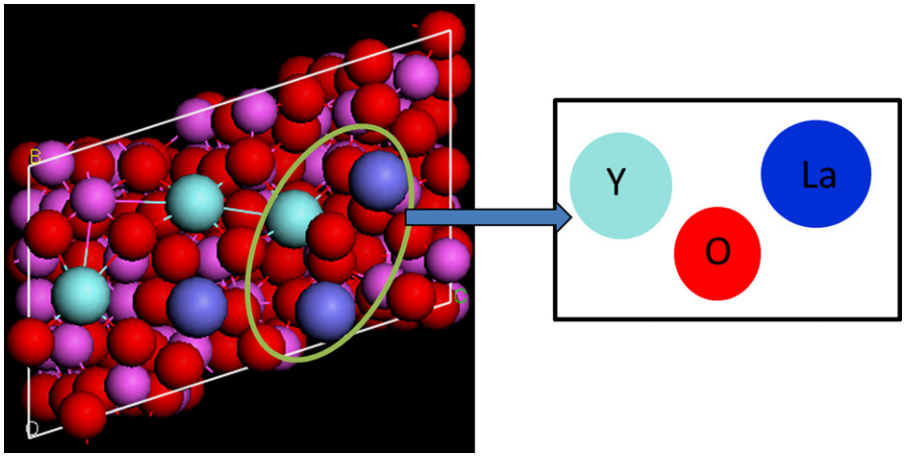

Fig. 10. (11.1) Y–La codoped surface looked from the top perpendicular to the surface. Specific coordinative arrangement/coupling effect where oxygen ion is always surrounded by two different types of dopant ions.

Table 6
Dopant–oxygen coordination number (CN) and nearest neighbor (NN) distance for different codoping combinations.

Doping combination	La–O		Mg–O		Y–O	
	CN	NN (Å)	CN	NN (Å)	CN	NN (Å)
La–Y surfaces	5.12–5.84	2.39–2.47	–	–	5.62–5.87	2.24–2.33
La–Y GB's	6.56–9.39	2.49–2.55	–	–	6.24–7.86	2.28–2.41
La–Mg surfaces	5.37–5.80	2.42–2.49	4.40–5.58	2.03–2.11	–	–
La–Mg GB's	7.49–7.80	2.49–2.53	5.12–5.97	2.11–2.14	–	–
Mg–Y surfaces	–	–	4.20–5.49	2.00–2.12	4.90–5.70	2.19–2.31
Mg–Y GB's	–	–	5.44–5.74	2.03–2.11	6.17–7.34	2.25–2.34
Single doped surfaces [23,24]	3.8–6.0	2.33–2.43	–	–	3.00–5.82	2.00–2.37
Single doped GB's [23,24]	5.5–6.5	2.36–2.45	5.00–5.50	2.09–2.12	6.51–7.49	2.30–2.40

single doped and codoped structures is observed. The coordination numbers as well as the nearest neighbor distance are similar in single doped and codoped alumina for Mg and Y. However, the Y–O coordination number seems to be more homogeneous than single doped alumina across different surfaces. For La–O on the other hand, the coordination numbers are significantly higher in codoped alumina in comparison to single doped alumina, which results in ordered and better packed structure of codoped grain boundaries in comparison to single doping as shown in Fig. 9. Observing no favorable interactions earlier in the segregation energy discussion, it can be said that La–Y codoping effect is a solid solution effect rather than being an energetic effect. These packed atomistic structure should strengthen the grain boundary against creep as also reported by Buban et al. [11]

3. Conclusions

Atomistic arrangements and segregation energies have been investigated using potential based energy minimization techniques for 9 different surfaces and 8-grain boundaries for La–Y codoping in alpha alumina. A lower number of surfaces and grain boundaries were investigated for the Mg–La and Mg–Y cases due to the higher computational cost caused by the need to introduce oxygen vacancies to compensate for the difference in valence of Mg with the host cation Al. Energy of segregation is negative for all the interfaces and for all the single doping and codoping combinations, which suggests that segregation of dopants is energetically favorable for all larger size dopant cations. Cosegregation does not have significant gain energetically over single doping in case of La–Y codoping. However, Y–Y, La–La and Y–La coordination number calculations in combination with atomistic structure of dopants show a preferred atomic arrangement of the dopant atoms (coupling effect) at the Y–La codoped interfaces. Segregation energy is more negative for Mg–La and Mg–Y codoping in comparison to single doping for most of the surfaces and grain boundaries, which may be attributed to two possible factors: grain boundary space created due to oxygen vacancies and disparity in the ionic size of the dopants. This observation leads to an interesting possibility of doping alumina with three different sized cations, e.g. Mg–La–In or La/Y–In, to further enhance the additional effects of codoping in alumina. For all the three cases, codoping results in an increase in the configurational entropy as well as the ordering of the atomistic structure in comparison to single doping, which will lead to strengthening of grain boundaries against creep.

Appendix A. Supplementary data

Supplementary data associated with this article can be found, in the online version, at doi:10.1016/j.jeurceramsoc.2012.02.056.

References

1. Robert Coble, Transparent alumina and method of preparation (United States Patent Office, March 20, 1962), http://www.google.com/patents?id=6NRtAAAAEBAJ&dq=3026210.
2. Kim B-N, Hiraga K, Morita K, Yoshida H, Miyazaki T, Kagawa Y. Microstructure and optical properties of transparent alumina. *Acta Materialia* 2009;**57**(5):1319–26.
3. Apetz Rolf, Bruggen Michel PB. Transparent alumina: a light-scattering model. *Journal of the American Ceramic Society* 2003;**86**(3):480–6.
4. Stuer Michael, Zhao Zhe, Aschauer Ulrich, Bowen Paul. Transparent polycrystalline alumina using spark plasma sintering: Effect of Mg, Y and La doping. *Journal of the European Ceramic Society* 2010;**30**(April (6)):1335–43.
5. Krell A, Blank P, Ma H, Hutzler T, Bruggen MPB, Apetz R. Transparent sintered corundum with high hardness and strength. *Journal of the American Ceramic Society* 2003;**86**(1):12–8.
6. Krell A, Blank P, Ma H, Hutzler T, Nebelung M. Processing of high-density submicrometer Al_2O_3 for new applications. *Journal of the American Ceramic Society* 2003;**86**(4):546–53.
7. Wei GC. Transparent ceramic lamp envelope materials. *Journal of Physics D: Applied Physics* 2005;**38**(September (17)):3057–65.
8. Peelen JGJ, Metselaar R. Light scattering by pores in polycrystalline materials: transmission properties of alumina. *Journal of Applied Physics* 1974;**45**(1):216.
9. Fang J, Thompson AM, Harmer MP, Chan HM. Effect of yttrium and lanthanum on the final-stage sintering behavior of ultrahigh-purity alumina. *Journal of the American Ceramic Society* 1997;**80**(8):2005–12.
10. Fabris S, Elsässer C. First-principles analysis of cation segregation at grain boundaries in α-Al_2O_3. *Acta Materialia* 2003;**51**(January (1)):71–86.
11. Buban JP, Matsunaga K, Chen J, Shibata N, Ching WY, Yamamoto T, et al. Grain boundary strengthening in alumina by rare earth impurities. *Science* 2006;**311**(January (5758)):212–5.
12. Li Yan-Zun, Wang Chongmin, Chan Helen M, Rickman Jeffrey M, Harmer Martin P, Chabala Jan M, et al. Codoping of alumina to enhance creep resistance. *Journal of the American Ceramic Society* 1999;**82**(6):1497–504.
13. Lartigue S, Priester L, Dupau F, Gruffel P, Carry C. Dislocation activity and differences between tensile and compressive creep of yttria doped alumina. *Materials Science and Engineering A* 1993;**164**(1–2):211–5.
14. Lartigue-Korinek S, Carry C, Priester L. Multiscale aspects of the influence of yttrium on microstructure, sintering and creep of alumina. *Journal of the European Ceramic Society* 2002;**22**(September (9–10)):1525–41.
15. Song H, Coble RL. Morphology of platelike abnormal grains in liquid-phase-sintered alumina. *Journal of the American Ceramic Society* 1990;**73**(7):2086–90.
16. Song Huesup, Coble Robert L. Origin and growth kinetics of platelike abnormal grains in liquid-phase-sintered alumina. *Journal of the American Ceramic Society* 1990;**73**(7):2077–85.
17. Swiatnicki W, Lartigue-Korinek S, Laval JY. Grain boundary structure and intergranular segregation in Al_2O_3. *Acta Metallurgica Et Materialia* 1995;**43**(2):795–805.
18. Elsässer Christian, Elsässer Traude. Codoping and grain-boundary cosegregation of substitutional cations in α-Al_2O_3: a density-functional-theory study. *Journal of the American Ceramic Society* 2005;**88**(1):1–14.
19. Gavrilov Konstantin L, Bennison Stephen J, Mikeska Kurt R, Chabala Jan M, Levi-Setti Riccardo. Silica and magnesia dopant distributions in alumina by high-resolution scanning secondary ion mass spectrometry. *Journal of the American Ceramic Society* 1999;**82**(4):1001–8.
20. Dillon Shen J, Harmer Martin P, Rohrer Gregory S. Influence of interface energies on solute partitioning mechanisms in doped aluminas. *Acta Materialia* 2010;**58**(September (15)):5097–108.
21. Cho J, Rickman Jeffrey M, Chan Helen M, Harmer Martin P. Modeling of grain-boundary segregation behavior in aluminum oxide. *Journal of the American Ceramic Society* 2000;**83**(2):344–52.
22. Cho J, Wang CM, Chan HM, Rickman JM, Harmer MP. Role of segregating dopants on the improved creep resistance of aluminum oxide. *Acta Materialia* 1999;**47**(15):4197–207.
23. Galmarini S, Aschauer U, Bowen P, Parker SC. Atomistic simulation of Y-doped α-alumina interfaces. *Journal of the American Ceramic Society* 2008;**91**(11):3643–51.
24. Galmarini S, Aschauer U, Tewari A, Aman Y, Van Gestel C, Bowen P. Atomistic modeling of dopant segregation in α-alumina ceramics: coverage

dependent energy of segregation and nominal dopant solubility. *Journal of the European Ceramic Society* 2011;**31**(December (15)):2839–52.
25. Aschauer U, Bowen P, Parker SC. Atomistic modeling study of surface segregation in Nd:YAG. *Journal of the American Ceramic Society* 2006;**89**(12):3812–6.
26. Aschauer U, Bowen P, Parker SC. Surface and mirror twin grain boundary segregation in Nd:YAG: an atomistic simulation study. *Journal of the American Ceramic Society* 2008;**91**(8):2698–705.
27. Watson Graeme W, Toby Kelsey E, Leeuw Nora H de, Harris Duncan J, Parker Stephen C. Atomistic simulation of dislocations, surfaces and interfaces in MgO. *Journal of the Chemical Society Faraday Transactions* 1996;**92**(January (3)):433–8.
28. Dick BG, Overhauser AW. Theory of the dielectric constants of alkali halide crystals. *Physical Review* 1958;**112**(October (1)):90–103.
29. Lewis GV, Catlow CRA. Potential models for ionic oxides. *Journal of Physics C: Solid State Physics* 1985;**18**(February (6)):1149–61.
30. Liu RS, Shi WC, Cheng YC, Huang CY. Crystal structures and peculiar magnetic properties of α- And γ-Al2O3 powders. *Modern Physics Letters B* 1997;**11**(26–27):1169–74.
31. Lizarraga Raquel, Holmstrom Eric, Parker Stephen C, Arrouvel Corinne. Structural characterization of amorphous alumina and its polymorphs from first-principles XPS and NMR calculations. *Physical Review B* 2011;**83**(March (9)):094201.
32. Mackrodt William C, Tasker Phillip W. Segregation isotherms at the surfaces of oxides. *Journal of the American Ceramic Society* 1989;**72**(9): 1576–83.
33. Cho Junghyun, Chan Helen M, Harmer Martin P, Rickman JM. Influence of yttrium doping on grain misorientation in aluminum oxide. *Journal of the American Ceramic Society* 1998;**81**(November (11)):3001–4.
34. Dillon SJ, Harmer MP. Demystifying the role of sintering additives with 'complexion'. *Journal of the European Ceramic Society* 2008;**28**(7):1485–93.